Journal of Sound and Vibration (2001) **241**(5), 755–777
doi:10.1006/jsvi.2000.3317, available online at http://www.idealibrary.com on IDEAL®

ACTIVE CONSTRAINED LAYER DAMPING OF CLAMPED-CLAMPED PLATE VIBRATIONS

C. Chantalakhana and R. Stanway

*Department of Mechanical Engineering, University of Sheffield, Mappin Street, Sheffield S*1 3*JD, England. E-mail: r.stanway@sheffield.ac.uk*

(*Received* 6 *July* 1999, *and in final form* 10 *July* 2000)

Surface damping treatments are often effective at suppressing higher frequency vibrations in thin-walled structures such as beams, plates and shells. However, the effective suppression of lower frequency modes usually requires the addition of an active vibration control scheme to augment the passive treatment. Advances in the technologies associated with the so-called smart materials are dramatically reducing the cost, weight and complexity of active structural control and make it feasible to consider active schemes in an increasing number of applications.

In this paper, the authors present a numerical and experimental study of the application of active constrained layer damping to a clamped–clamped plate. Specifically, a passive constrained viscoelastic damping layer is augmented with an active scheme employing a PZT patch as the actuator. In the opening sections of the paper, emphasis is placed upon establishing a suitable model of the plate. Starting with an established finite element formulation it is shown how model updating and model reduction are required to produce a low order state-space model which can be used as the basis for active control. The effectiveness of the formulation is then demonstrated in a numerical study. Finally, in the description of the experimental study, it is shown how modes in the frequency range from 0 to 600 Hz are effectively suppressed: the two lowest modes (bending and torsional) through active control using only a single sensor and single actuator in the feedback loop, the higher modes (around 10 in number) by the constrained passive damping layer. The paper's original contribution lies in the experimental demonstration that given a sufficiently accurate model of the plate and passive constrained damping layer, together with a suitable active feedback control algorithm, spillover effects are not significant even when using a single sensor and single actuator. The experimental traces show, in some instances, minor effects due to spillover. However, it can be concluded that the presence of the passive layer introduces sufficient damping into the residual modes to avoid any major problems when using only the minimum amount of active control hardware.

1. INTRODUCTION

The application of active control techniques to suppress vibrations in flexible structures poses some special problems. These problems arise primarily from the distributed nature of such structures and the resulting large number of degrees of freedom which are required in a mathematical model to account for observed behaviour. If a lumped parameter model is derived then this generally needs to be reduced in order prior to controller design. Balas [1] investigated the so-called spillover effects which result from ignoring higher order modes when implementing active feedback control. It was shown that spillover effects are liable to degrade or even de-stabilize the response of the closed-loop system. Various techniques for reducing the influence of spillover effects have been proposed. One effective technique in

0022-460X/01/150755 + 23 $35.00/0

which modal transformations were employed so as to control each mode independently was described by Meirovitch and his colleagues [2]. It was demonstrated that no spillover occurs if the number of actuators is equal to the order of the lumped parameter model and the number of sensors is capable of identifying all of the controlled modes. Furthermore, the performance of the so-called independent modal-space control (IMSC) was shown to be superior in almost every respect to techniques which seek to exploit the coupling in a flexible structure in order to minimize the number of actuators and sensors. Unfortunately, the hardware requirements for the independent control of modes can be daunting and alternative techniques have been investigated with the aim of reducing spillover effects whilst also reducing the number of actuators and sensors.

Early attempts at achieving these joint aims almost invariably involved experiments using various cantilevered beams with piezoelectric elements to implement the control. Bailey and Hubbard [3] overcame spillover effects by employing a distributed parameter control algorithm. A drawback with this method concerned the need to provide a measurement of the angular velocity of the beam's tip. Since such a measurement was not available the experiments were limited to control of the fundamental mode. An alternative approach was proposed by Fanson and Caughey [4]. These authors described experiments to control the first six bending modes of a cantilevered beam using the so-called positive position feedback (PPF). It was shown that using PPF the effect of spillover is to stabilize rather than de-stabilize the closed-loop system. In a further example involving a cantilevered beam, Baz and his colleagues [5] showed how the attributes of IMSC and PPF could be combined to provide effective real-time control of structural vibrations using a smaller number of actuators.

In the early 1990s, reports began to appear of an alternative approach to controlling structural vibrations: using active techniques to augment the damping provided by a passive constrained layer added to the host structure. It had long been recognized that passive constrained layer damping is most effective at suppressing vibrations of the higher frequency modes. Using a hybrid approach, it appeared feasible to use active control to suppress the lower modes while the passive layer would reduce spillover from the higher frequency modes. Baz and Ro [6] demonstrated the feasibility of this concept using the ubiquitous cantilevered beam but soon progressed to more complex structures such as plates and shells. Using a cantilevered plate, partially treated with an active constrained damping layer, Baz and Ro [7] showed how the bending mode could be controlled effectively using a simple proportional control arrangement. A comparison of active, passive and hybrid (i.e., active constrained layer damping treatments) appeared in the study by Veley and Rao [8]. A cantilevered beam and also a plate clamped on all four sides were used as host structures to examine and compare active, passive and hybrid control strategies. The design objectives were to minimize the weight of the structures and also to achieve high levels of damping. The results showed that the hybrid approach is superior to the active control of an untreated plate in that a given damping ratio can be achieved using less than half the mass.

The present study is concerned with a clamped–clamped aluminium plate which was first investigated by Azvine and his colleagues [9]. This plate is a simplified version of an instrument box cover found in a military aircraft. Azvine's brief was to investigate active constrained layer damping treatments as a means of suppressing bending and torsional vibrations which were causing the instrument box to malfunction in service. Negative velocity feedback was used along with non-collocated sensors and actuators in an attempt to control the first two modes of vibration. Using two actuators, the benefits of the constraining layer were clearly demonstrated: higher feedback gains could be used to give lower resonant peaks without causing instability. However, this study indicated the need for

better models of the host plate, the passive constraining layer and the piezoelectric actuators together with a more effective control algorithm based upon this model. At the same time, it was essential for the eventual application that the amount of hardware be minimized. Consequently, in the present investigation, it was decided to investigate whether effective control could be achieved using only a single actuator and single sensor.

In what follows here, the authors describe this novel approach to controlling both the bending and torsional vibrations of the clamped–clamped plate. Initially, the technique of Baz and Ro [7] is extended to produce a finite element model of the plate together with the passive constraining layer. Using system identification techniques, the model is validated using data from the test facility. Model reduction and model updating are then applied to produce a compact model which is capable of accounting for observed behaviour. Following a comprehensive numerical study, active constrained layer damping treatments is implemented experimentally and a comprehensive set of test results is presented.

2. FINITE ELEMENT MODELLING

2.1. STRATEGY

The strategy adopted by the authors is to develop a model-based approach to the investigation of active constrained layer damping of a clamped–clamped plate. Modelling of the plate and its passive damping treatment is conveniently performed using finite element analysis in order to determine the equations of motion in terms of mass, damping and stiffness matrices. Active control is more conveniently formulated in state-space notation which requires transformation of the finite element model [10]. This transformation is straightforward in principle but can be difficult in practice. The choice of model order is crucial if observed behaviour is to be accounted for without requiring excessive matrix dimensions. To obtain an acceptable compromise, formal model reduction techniques [11] will be used here. Also, it has been found necessary to use model updating algorithms [12] in order to obtain sufficiently close correspondence between model predictions and observed behaviour.

2.2. MATHEMATICAL MODEL

The system under consideration involves the host plate to which is added a viscous elastic layer and a further metallic constraining layer. The modelling technique follows Khuata and Cheung [13] and Baz and Ro [7]. Rectangular plate elements are used as shown in Figure 1. The co-ordinate system is illustrated in Figure 1(a) and the displacements in Figure 1(b). The analysis of the host plate and the metallic constraining layer employs the assumptions of thin-plate theory that can be found in any suitable textbook on fundamental plate theory or finite element analysis, for example, Dawe [14]. In addition, it is assumed that a plane section of the viscoelastic layer remains plane after deformation, and that there is no shear strain in the constraining layer and host plate. At each node k of element j, there are seven degrees of freedom, four longitudinal, one transverse and two rotational displacements. These displacements can be gathered together to form a vector:

$$\mathbf{\Delta}_j = \left\{ u_{1k}, v_{1k}, u_{3k}, v_{3k}, w_k, \frac{\mathrm{d}w}{\mathrm{d}y_k}, \frac{\mathrm{d}w}{\mathrm{d}x_k} \right\}^{\mathrm{T}}, \quad k = 1, 2, 3, 4, \tag{1}$$

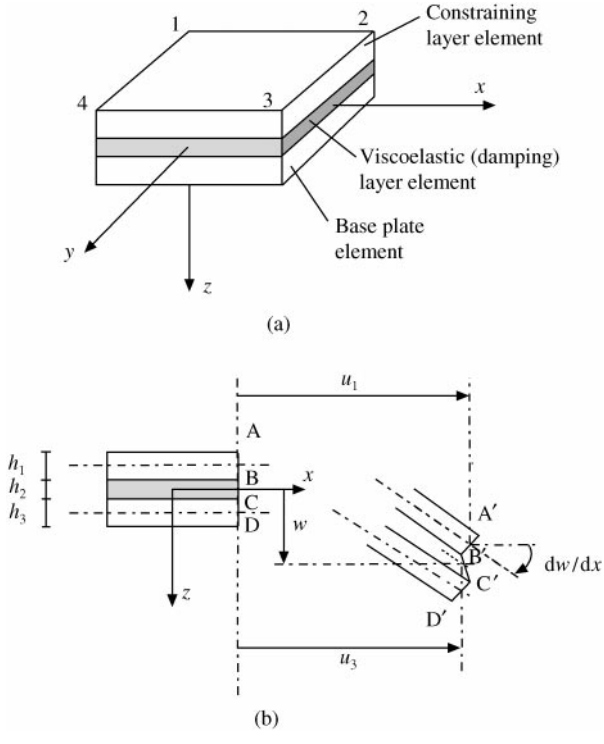

Figure 1. A rectangular element of the three-layer plate: (a) co-ordinate system and nodes of the elements; (b) displacement of the elements at x–z plane.

where u_{1k}, v_{1k} and u_{3k}, v_{3k} are longitudinal displacements of the constraining layer and base plate, respectively, in the x–z and y–z planes. Given this displacement vector, the equation of motion is formed as

$$\mathbf{M}_j \ddot{\mathbf{\Delta}}_j + \bar{\mathbf{K}}_j \mathbf{\Delta}_j = \mathbf{F}_j, \tag{2}$$

where $\mathbf{M}_j$ and $\bar{\mathbf{K}}_j$ are, respectively, the mass and stiffness matrices of element j and $\mathbf{F}_j$ is an external force vector acting at the jth element. The arrays $\mathbf{M}_j$ and $\bar{\mathbf{K}}_j$ are formulated by the strain energy method [7, 13]. The shear modulus of the viscoelastic damping material is given by $G(1 + i\eta)$ where G is the shear modulus and η is the loss factor which is frequency dependent. Consequently, $\bar{\mathbf{K}}$ is a complex stiffness matrix whose imaginary part serves as a loss energy or damping term. Full details (including experimental validation) of this finite element plate model are given in reference [15].

3. PASSIVE CONTROL OF PLATE VIBRATIONS

The plate used originates from a vibration control problem described by Azvine and his colleagues [9]. In the present investigation, the original panel is modelled as a plate clamped along opposite edges.

The plate is aluminium and has the dimensions 2·5 mm × 305 mm × 490 mm. The experimental arrangement of the clamped–clamped plate is shown in Figure 2. Preliminary experiments indicated that given excitation and measurement points at node 7, the first 10 modes can be excited and detected. These modes will be identified experimentally and

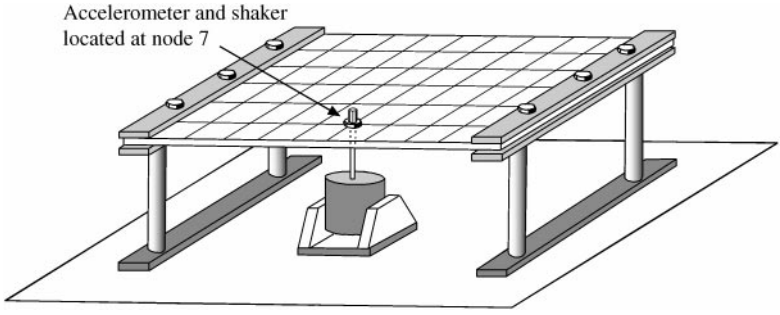

Figure 2. Experimental arrangement of the clamped–clamped plate for passive constrained layer damping experiments.

compared with model predictions before consideration of model updating. Passive damping, through the addition of viscoelastic and constraining layers, must aim to attenuate levels of plate vibration. Ross and his colleagues [16] provided guidelines for designing suitable surface treatments for plates. In the present study, self-adhesive damping tape is used in conjunction with a thin metallic constraining layer. To simplify the calculation of the damping properties, the relationship between the damping and constraining layers is assumed to obey the relationship [16]

$$0{\cdot}05 < 2h_{23} + h_{13} < 0{\cdot}15, \tag{3}$$

where h_{23} and h_{13} are, respectively, the ratios of the damping and constraining layer thicknesses to the base-plate thickness. The maximum loss factor introduced as a result of the damping treatment can be calculated from [16]

$$\eta_{\max} = \frac{3{\cdot}5e_{13}h_{13}}{2 + 3{\cdot}5e_{13}h_{13}} \times \frac{\eta}{(1 + \sqrt{1 + \eta^2})}, \tag{4}$$

where e_{13} is the ratio of the modulus of elasticity of the constraining layer to that of the base plate (or E_1/E_3). It is stated in reference [16] that the maximum error from this approximate solution is 15%. There are four parameters to choose in the design process, the two parameters h_2, thickness, and η, loss factor for the damping layer and the two parameters h_1, thickness, and E_1, modulus of elasticity for the constraining layer. Equation (4) implies that the maximum damping is proportional to the loss factor η of the damping layer and the thickness and modulus of elasticity of the constraining layer with respect to the fixed values of the base-plate thickness h_3 and modulus of elasticity E_3. From commercially available materials, a 50·8 μm (0·002 in) thick ISD112 viscoelastic layer from the 3M company was selected from the manufacturer's data sheet to provide a loss factor of approximately 1·0 in the frequency range from 0 to 600 Hz. A 0·254 mm (0·010 in) thick steel shim was used as the constraining layer giving an upper limit (equation (3)) equal to 0·1422. The steel shim was used to provide a high modulus of elasticity for the constraining layer. Table 1 gives the material properties for all three layers.

Figure 3 shows the influence of the passive constrained damping layer when compared with the response of the undamped host plate. Note that the introduction of the damping layer produces around 25 dB attenuation of all the modes up to 600 Hz. However, the vibrations associated with the first two modes still produce mobility peaks some 20 dB above those associated with the higher modes. It is these first two modes, one bending and

TABLE 1

Material properties of three-layer plate

Material	Modulus of elasticity (MPa)	Modulus of rigidity (MPa)	Density (kg/m^3)	Poisson's ratio	Shear loss factor
Aluminium plate	70×10^3	—	2700	0·3	—
ISD112 viscoelastic layer	29·8†	20†	1140	0·49	1·0†
Steel constraining layer	200×10^3	—	7000	0·3	—

†At the centre frequency of 600 Hz.

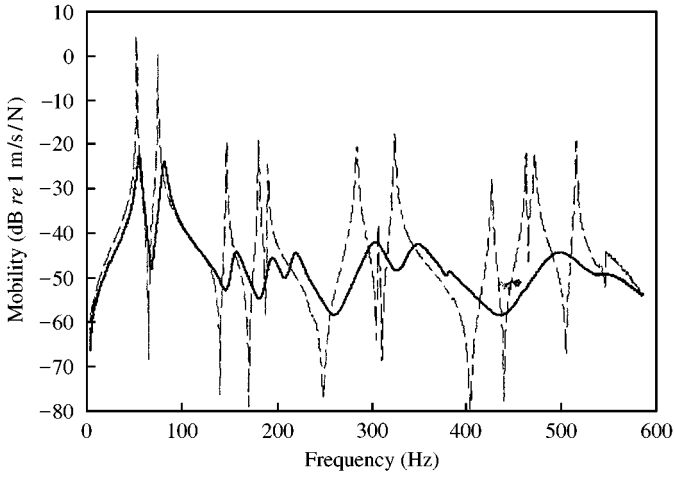

Figure 3. Measured FRFs of the panel plate with and without constrained damping layer: - - - -, without passive damping layer; ———, with passive damping layer.

one torsion, which require the use of active control to introduce significant additional attenuation of vibration levels. Before proceeding to describe active constrained layer damping it is necessary to refine the finite element model of the passively damped plate. A comparison between the predicted frequency response function (FRF) from the finite element model and the FRF measured experimentally (Figure 4), shows that the response levels predicted by the model are consistent with the results from the experiments. However, there are discrepancies in the predicted natural frequencies. The discrepancies in natural frequencies probably stem from imperfect clamping at the two ends (see Figure 2) where rotational stiffness is present. These discrepancies will be minimized using updating techniques before the model is used for control system design.

4. MODEL UPDATING

In the FRFs shown in Figure 4, the FRF predicted by the finite element model is shifted to the right of the experimental FRF. A pole placement technique was used to update the finite element model so that both the predicted natural frequencies and modal damping factors are modified so as to match the experimentally measured data.

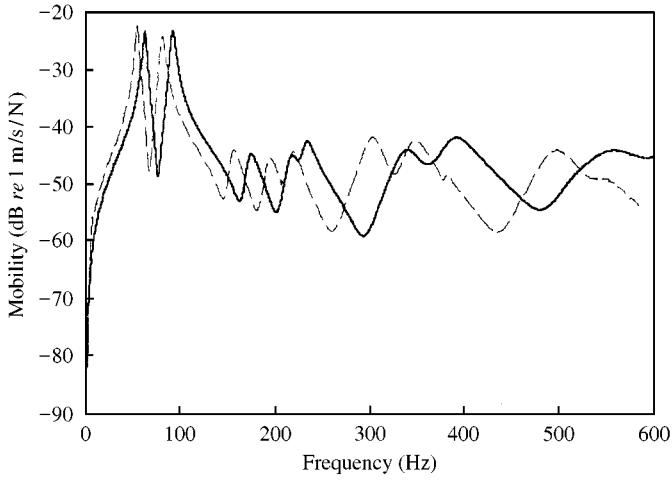

Figure 4. Measured and predicted FRFs (point mobility, the same point for acting force and velocity response) of the panel plate covered with constrained damping layer: ----, measured FRF; ——, predicted FRF.

4.1. SUMMARY OF POLE PLACEMENT TECHNIQUE

One updating algorithm using a pole placement technique was described by Inman and Minas [17]. Stiffness and damping matrices in the equation of motion are updated to match the identified natural frequencies and damping factors produced by experimental testing. A brief review of the technique is necessary in order to understand the transformation of equation (2) which is required before updating can be performed.

Consider the state-space form of the equations of motion [10],

$$\begin{Bmatrix} \ddot{\mathbf{\Delta}} \\ \dot{\mathbf{\Delta}} \end{Bmatrix} = \begin{bmatrix} -\mathbf{M}^{-1}\mathbf{D} & -\mathbf{M}^{-1}\mathbf{K} \\ \mathbf{I} & \mathbf{0} \end{bmatrix} \begin{Bmatrix} \dot{\mathbf{\Delta}} \\ \mathbf{\Delta} \end{Bmatrix} + \begin{bmatrix} \mathbf{B}_0 \\ \mathbf{0} \end{bmatrix} \mathbf{f}, \tag{5}$$

where $\mathbf{D}$ is an $(n \times n)$ damping matrix, $\mathbf{I}$ is an $(n \times n)$ identity matrix, $\mathbf{B}_0$ is an $(n \times n)$ input matrix and $\mathbf{f}$ is an $(n \times 1)$ input vector. If the vector $\mathbf{f}$ is used to provide the feedback signal, then

$$\mathbf{f} = \mathbf{GC} \begin{Bmatrix} \dot{\mathbf{\Delta}} \\ \mathbf{\Delta} \end{Bmatrix}, \tag{6}$$

where $\mathbf{G}$ is an $(n \times 2m)$ gain matrix, $\mathbf{C}$ is an $(2m \times 2n)$ measurement matrix containing $2m$ rows of eigenvectors and m is the number of modes to be updated. Note that these modes occur as complex conjugate pairs. A method of calculating the elements of $\mathbf{G}$ is given by Porter and Crossley [18]. A suitable choice of the matrix $\mathbf{B}_0$ to provide controllability of all the modes is the identity matrix $\mathbf{I}$ [17]. Then the second term on the right-hand side of equation (5) acts as a correction term and equation (5) can be rewritten as

$$\begin{Bmatrix} \ddot{\mathbf{\Delta}} \\ \dot{\mathbf{\Delta}} \end{Bmatrix} = \begin{bmatrix} -\mathbf{M}^{-1}\mathbf{D} & -\mathbf{M}^{-1}\mathbf{K} \\ \mathbf{I} & \mathbf{0} \end{bmatrix} \begin{Bmatrix} \dot{\mathbf{\Delta}} \\ \mathbf{\Delta} \end{Bmatrix} + \begin{bmatrix} \mathbf{\Delta A}_1 & \mathbf{\Delta A}_2 \\ \mathbf{0} & \mathbf{0} \end{bmatrix} \begin{Bmatrix} \dot{\mathbf{\Delta}} \\ \mathbf{\Delta} \end{Bmatrix} \tag{7}$$

where $\mathbf{\Delta A}_1$ and $\mathbf{\Delta A}_2$ are the $(n \times n)$ mass-normalized correction matrices of the damping and stiffness matrices, respectively, and are obtained from the inner product of $\mathbf{B}_0(\mathbf{GC})$. Define

$\mathbf{A}_1 = -\mathbf{M}^{-1}\mathbf{D} + \Delta\mathbf{A}_1$ and $\mathbf{A}_2 = -\mathbf{M}^{-1}\mathbf{K} + \Delta\mathbf{A}_2$, then the updated damping and stiffness matrices can be obtained from

$$\mathbf{D}_{new} = -\mathbf{M}\mathbf{A}_1, \qquad \mathbf{K}_{new} = -\mathbf{M}\mathbf{A}_2, \tag{8}$$

where $\mathbf{D}_{new}$ and $\mathbf{K}_{new}$ are the updated damping and stiffness matrices respectively. In equation (7), it is assumed that the damping matrix $\mathbf{D}$ represents viscous damping. Consequently, it is necessary to transform the imaginary term of the complex stiffness matrix of the plate model as formulated in equation (2) to an equivalent viscous damping matrix.

4.2. TRANSFORMATION OF THE IMAGINARY TERM OF THE COMPLEX STIFFNESS MATRIX TO AN EQUIVALENT VISCOUS DAMPING MATRIX

The imaginary term of the complex stiffness matrix can be transformed to approach the viscous damping matrix where the viscous damping coefficients are now frequency dependent. The algorithm used to achieve this damping transformation is adapted from work by Minas and Inman [19] and was originally used for identifying a non-proportional damping matrix from experimental data. Details of the transformation have been presented by Chantalakhana and Stanway [15]. Although this transformation is straightforward in principle, difficulties in the present application arise owing to the dimensions of the matrices, which are involved. Essentially, the pseudo-inverse of an overdetermined system of linear equations incorporating a $(2n^2 \times (n^2 + n)/2)$ order matrix needs to be computed. Consequently, the mass and complex stiffness matrices of the finite element plate model need to be reduced in size. To overcome this problem, the authors used the Guyan reduction technique [20] to reduce the order of system equations before implementing the transformation.

4.3. VALIDATION OF THE UPDATED MODEL

In this section, the pole placement algorithm for updating the model is implemented in order to study its performance. Experimental data are required to implement the algorithm. The diagram in Figure 5 summarizes the procedures necessary to achieve a refined, reduced order model of the three-layer plate.

4.3.1. *Tentative model*

Details of the first three stages in implementing the flow-chart in Figure 5 are described below. The finite element model is obtained by discretizing the three-layer plate as 9×6 elements along the length and width directions, respectively, as shown in Figure 6.

The number of degrees of freedom n of the original finite element plate model is 420. Guyan reduction is performed by maintaining the transverse displacements of selected nodes (see Figure 6) and the longitudinal displacements of the constraining layer at four selected nodes. These nodes will be used in the active control strategies which are described later. In this way, the number of degrees of freedom is reduced from $n = 420$ to $r = 36$. The selection of these master nodes needs to ensure a suitable reduced order model over the bandwidth of interest and also maintain correspondence with the measurement points used in the experimental procedures. Guidelines for this node selection can be found in Shah and Raymund [21]. The equation of motion with reduced mass and complex stiffness matrices is

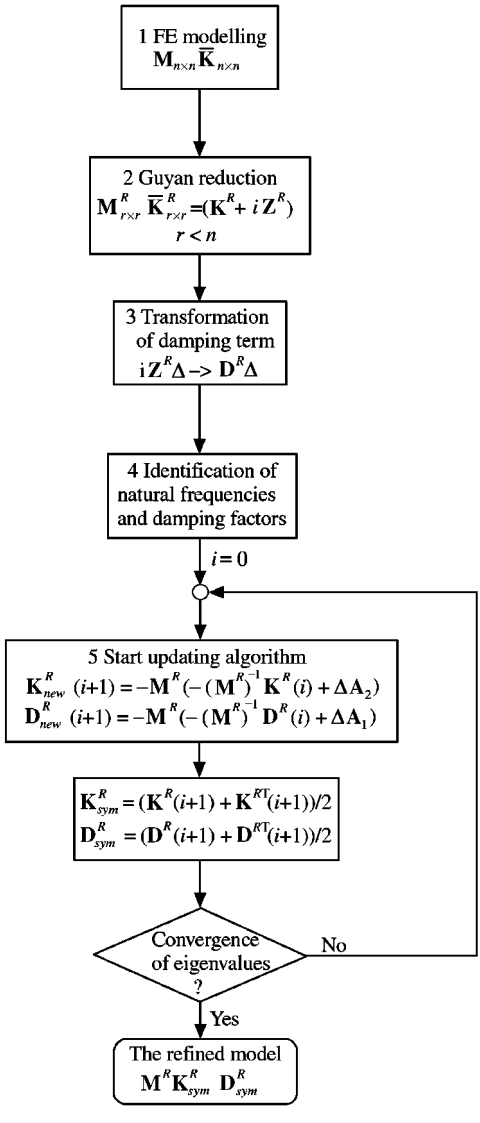

Figure 5. Procedures to achieve the refined model constructed using finite element analysis.

then solved to obtain the eigensolutions. These solutions are then used to transform the imaginary term $\mathbf{Z}^R$ of the reduced complex stiffness matrix $\bar{\mathbf{K}}^R$ to an $(r\times r)$ equivalent viscous damping matrix $\mathbf{D}^R$. The dynamic responses of this reduced order plate model deviate from the original model owing to ignorance of the inertia term in the transformation using Guyan reduction [22] and the pseudo-inverse used in the damping transformation algorithm. The reduced order model eventually will be updated with parameters identified from experiments in order to match the model predictions to the observed behaviour of the plate structure.

4.3.2. *Identification of natural frequencies and damping factors*

Identified natural frequencies and damping factors are used to update the finite element plate model. The frequency range of interest is from 0 to 600 Hz where modal damping

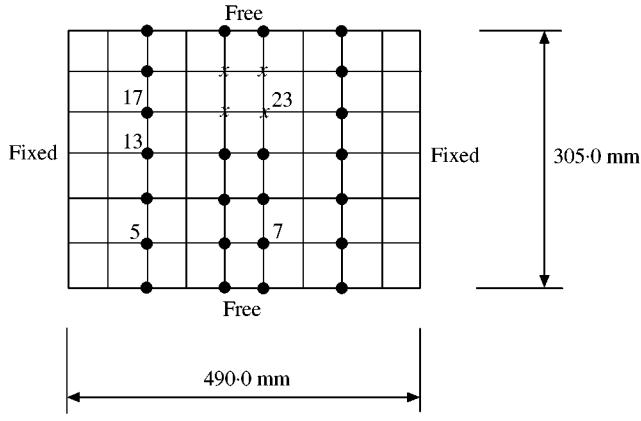

Figure 6. Division of plate to finite elements and selected nodes for model reduction. Selected nodes: ●, transverse motion; ×, transverse plus longitudinal motion.

TABLE 2

Measured and predicted first six natural frequencies and damping factors of three-layer plate

Mode	1	2	3	4	5	6
Predicted natural frequency (Hz)	62·50	92·23	172·93	217·07	233·02	339·06
Measured natural frequency (Hz)	54·53	81·50	157·47	195·59	220·60	304·02
Predicted % damping	3·50	3·05	3·81	3·87	2·83	4·86
Measured % damping	3·44	3·51	4·13	3·66	3·41	3·57

factors are generally less than 0·05. Hence, a simple peak picking method can be used for identification [23, 24]. Care must be taken when using the method since peak picking requires well-separated modes. Many plate configurations have coincident modes but this feature does not occur within the frequency range of interest of the plate used here. Note that, in Figure 3, mode 7 at around 300 Hz disappears when the passive layer is applied to the plate. Owing to the unavailability of mode 7, only the first six modes are identified. Table 2 gives the identified natural frequencies and percentage damping factors of the first 6 modes compared with those from the model predictions. Specifically, the predictions are obtained from the r order reduced model which is updated with the eigenvalues of the full n order plate model. Then the predicted natural frequencies and damping factors are the same for both models.

4.3.3. *Model updating iteration and refined model*

Unfortunately, the mass-normalized correction terms of the damping matrix ($\mathbf{\Delta A}_1$) and of the stiffness matrix ($\mathbf{\Delta A}_2$) are not guaranteed to be symmetrical such that the orthogonality properties of the modal model are satisfied [23]. These properties are required to enable decomposition of the system equations used in modal control. Because of the requirement for symmetrical stiffness and damping matrices, the updating procedures need to be repeated until the updated eigenvalues are acceptable when compared with the identified eigenvalues (see Figure 5). Figures 7 and 8 show a comparison of FRFs before and after updating the finite element three-layer plate model. The notation used is FRFj_k where j is

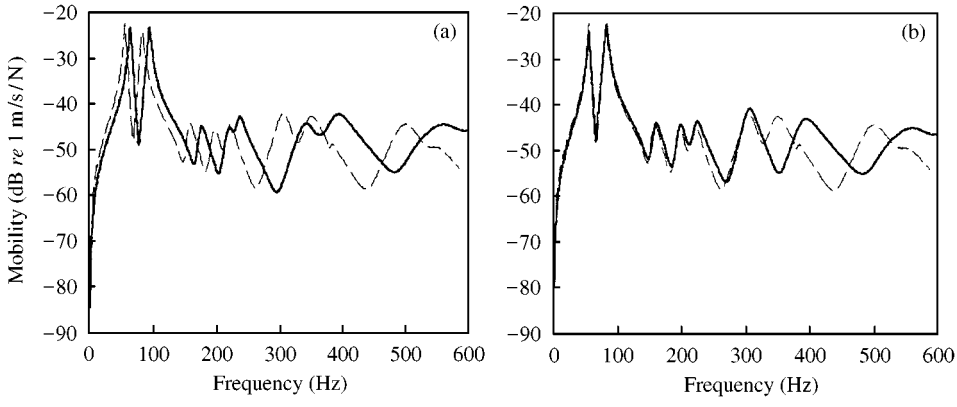

Figure 7. FRF7_7 (a) before updating; (b) after updating the model.

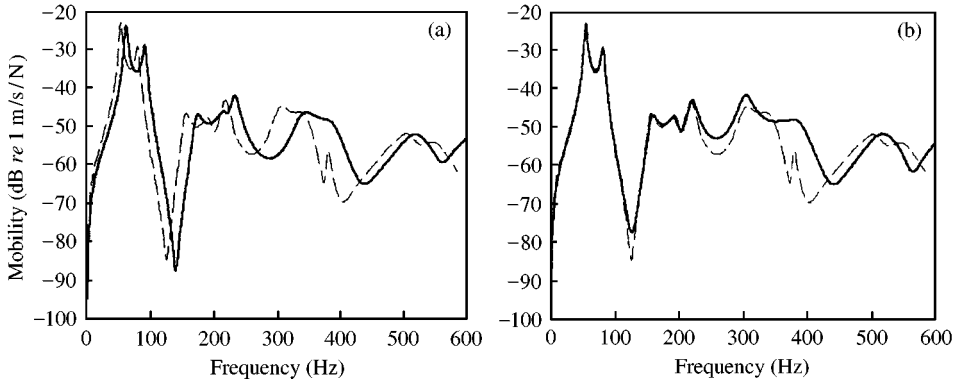

Figure 8. FRF7_23 (a) before updating; (b) after updating the model.

the excitation point and k is the measurement point as indicated in Figure 6. In Figures 7 and 8, the dashed lines represent the measured FRFs and the solid lines represent the FRFs from prediction (a) before updating and (b) after updating the model. These results clearly show that the first six modes of the predicted FRFs are concurrent with the measured FRFs and the higher modes (i.e., those not updated) are unchanged. Although mismatches of the higher modes are clearly present, the accuracy of the updated models is sufficient to use in an active design scheme where it is the accuracy of *controlled* pole locations which is required.

5. MODAL CONTROL

From the results in section 3 (Figures 3 and 4), the FRFs of the plate treated with a passive constrained damping layer show that an additional active control scheme is required to provide adequate attenuation the first two modes of vibration of the plate. An active element used to perform control action consumes energy and generally multiple sensors and actuators are required if multiple modes are to be controlled. In the present study, modal control theory [1] associated with coupling of the control force is used. An advantage of coupling the force is to control a number of modes simultaneously using the minimum number of actuators. However, spillover effects must obviously be taken into account.

5.1. MODAL STATE-SPACE FORM OF EQUATIONS OF MOTION

For the reduced order finite element plate model with r degrees of freedom, the corresponding state-space equation of motion is written as a set of $2r$ first order differential equations:

$$\begin{Bmatrix} \ddot{\mathbf{\Delta}} \\ \dot{\mathbf{\Delta}} \end{Bmatrix} = \begin{bmatrix} \mathbf{0} & \mathbf{M}^R \\ \mathbf{M}^R & \mathbf{D}^R \end{bmatrix}^{-1} \begin{bmatrix} \mathbf{M}^R & \mathbf{0} \\ \mathbf{0} & -\mathbf{K}^R \end{bmatrix} \begin{Bmatrix} \dot{\mathbf{\Delta}} \\ \mathbf{\Delta} \end{Bmatrix} + \begin{bmatrix} \mathbf{0} & \mathbf{M}^R \\ \mathbf{M}^R & \mathbf{D}^R \end{bmatrix}^{-1} \begin{Bmatrix} \mathbf{0} \\ \mathbf{F} \end{Bmatrix}, \tag{9}$$

where $\mathbf{\Delta}$ is an $(r \times 1)$ displacement vector, $\mathbf{M}^R$, $\mathbf{D}^R$ and $\mathbf{K}^R$ are $(r \times r)$ mass, damping and stiffness matrices, respectively, and $\mathbf{F}$ is an $(r \times 1)$ force vector acting at the nodal points. For the special case of a single input force, equation (9) may written in the form

$$\dot{\mathbf{Y}} = \mathbf{A}\mathbf{Y} + \mathbf{b}f \tag{10}$$

where $\mathbf{Y}_{2r\times 1} = [\dot{\mathbf{\Delta}}^{\mathrm{T}}\, \mathbf{\Delta}^{\mathrm{T}}]^{\mathrm{T}}$, $\mathbf{A}_{2r\times 2r}$ is a plant matrix, $\mathbf{b}_{2r\times 1}$ is an input vector and f is a scalar input. Let $\mathbf{Y} = \mathbf{U}\xi$, where $\xi_{2r\times 1}$ is a modal state variable vector and $\mathbf{U}_{2r\times 2r}$ is a transformation matrix containing $2r$ columns of the eigenvectors of $\mathbf{A}$. After substituting this transformation into equation (10) and pre-multiplying by $\mathbf{U}^{-1}$, then equation (10) becomes

$$\dot{\xi} = \mathbf{\Lambda}\xi + \mathbf{w}f, \tag{11}$$

where $\mathbf{\Lambda} = \mathbf{U}^{-1}\mathbf{A}\mathbf{U}$ is a diagonal matrix containing $2r$ eigenvalues of $\mathbf{A}$ along its diagonal elements, $\mathbf{w} = \mathbf{U}^{-1}\mathbf{b}$ is a modal controllability vector in which an element j of $\mathbf{w}$ quantifies controllability of the jth mode by the input f. This transformation results in the de-coupling of equation (10). If equation (11) is partitioned as c controlled mode equations and u residual or uncontrolled mode equations, then equation (11) can be re-arranged as

$$\begin{Bmatrix} \dot{\xi}_c \\ \dot{\xi}_u \end{Bmatrix} = \begin{bmatrix} \mathbf{\Lambda}_c & \mathbf{0} \\ \mathbf{0} & \mathbf{\Lambda}_u \end{bmatrix} \begin{Bmatrix} \xi_c \\ \xi_u \end{Bmatrix} + \begin{Bmatrix} \mathbf{w}_c \\ \mathbf{w}_u \end{Bmatrix} f. \tag{12}$$

The c controlled eigenvalues can be shifted to their desired values by feeding back the vector of state variables ξ_c, as a scalar input f with appropriate weightings

$$f = \mathbf{k}_c^{\mathrm{T}} \xi_c, \tag{13}$$

where $\mathbf{k}_c$ is a $(c \times 1)$ gain vector.

The scalar feedback input f in equation (13) is formed from the modal state variable vector ξ_c which needs to be computed from physical measurements. A state estimator [10] is implemented in conjunction with the modal controller to obtain estimates of all controlled state variables.

5.2. SPILLOVER EFFECTS

Balas [1] showed that using a reduced set of equations for the controller and estimator causes, respectively, control and observation spillover. A scalar input force f can excite the controllable residual modes (see equation (12)) because of the force coupling which is present. Similarly, if the measurement signal includes terms from the residual state variable ξ_u, then the estimator is contaminated by amplified noise. These spillover effects can cause instability in the controlled structure. However, these effects can be reduced by keeping the

elements of the control and estimator gain vectors low. Optimal designs such as the linear quadratic regulator and Kalman filter [25] can be used to achieve this. Placement of the actuator and sensor should be close to the nodal lines of residual modes so that the residual modes are not significantly excited and the residual state variables in ξ_u are not strongly observed.

6. DESIGN OF CONTROLLER

In what follows, the simplest possible configuration of sensor and actuator is considered: a single accelerometer and a single lead zirconate ceramic (PZT) actuator respectively. The state estimator and the control law are designed in the continuous-time domain and then transformed to the discrete-time domain for digital implementation. Placement of the sensor and the actuator are described below.

6.1. PLACEMENT OF SENSOR AND ACTUATOR

Plots of mode shapes are used to identify positions for the sensor and actuator such that they detect and excite the maximum transverse displacements of the first two modes whilst also keeping to the nodal lines of the higher modes so as to minimize spillover effects. The modal controllability and observability vectors are used to refine the selection of the sensor and actuator locations.

The first six mode shapes are considered and then the sensor and actuator are located in the middle of the upper half portion of the plate as illustrated in Figure 9. The dimensions of the PZT actuator are chosen based upon the results obtained by finite element modelling and experimental observations. A $50\,\text{mm} \times 50\,\text{mm}$ PZT patch is used as the actuator. Table 3 gives the controllability and observability indices of these sensor and actuator locations from the first six elements of the mode controllability vector $\mathbf{w}$ and the mode observability vector [10] respectively. Controllability and observability indices are low for modes 3 and 4 where the actuator and sensor are placed near their nodal lines, but are high for modes 1 and 2 where the actuator and sensor locations are in the region of maximum transverse motion so as to provide large induced shear strain in the damping layer.

6.2. CONTROL LAW AND ESTIMATOR DESIGN

For the state-space equations with a single input and single output (SISO), the control gain vector $\mathbf{k}_c^{\mathrm{T}}$ in equation (13) and estimator gain can be assigned using a pole placement

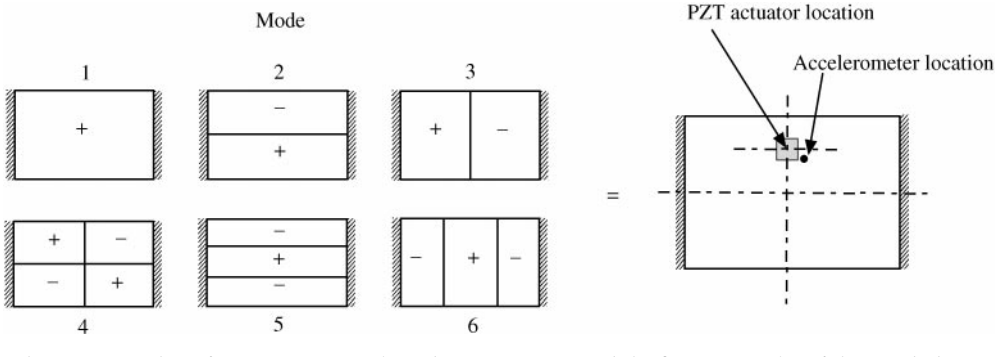

Figure 9. Location of PZT actuator and accelerometer to control the first two modes of the panel plate.

TABLE 3

Controllability and observability indices

Mode	Controllability	Observability
1	$6{\cdot}30 \pm 1{\cdot}060 \times 10^{1}i$	$-1{\cdot}145 \times 10^{-1} \pm 1{\cdot}557 \times 10^{-1}i$
2	$-5{\cdot}05 \pm 9{\cdot}09i$	$3{\cdot}66 \times 10^{-2} \pm 8{\cdot}67 \times 10^{-2}i$
3	$-1{\cdot}500 \times 10^{-8} \pm 7{\cdot}30 \times 10^{-8}i$	$-1{\cdot}442 \times 10^{-2} \pm 5{\cdot}16 \times 10^{-4}i$
4	$-5{\cdot}97 \times 10^{-8} \pm 3{\cdot}39 \times 10^{-8}i$	$-6{\cdot}15 \times 10^{-3} \pm 7{\cdot}94 \times 10^{-3}i$
5	$-8{\cdot}43 \times 10^{-1} \pm 2{\cdot}49 \times 10^{-1}i$	$-1{\cdot}256 \times 10^{-1} \pm 3{\cdot}53 \times 10^{-2}i$
6	$2{\cdot}16 \times 10^{2} \pm 2{\cdot}51 \times 10^{2}i$	$-2{\cdot}81 \times 10^{-2} \pm 1{\cdot}527 \times 10^{-2}i$

TABLE 4

Poles and gains of designed controller

Mode	Original poles (rad/s)	Desired poles (rad/s)	Control gain	Estimator gain
1	$-11{\cdot}78 \pm 343i$	$-105{\cdot}6 \pm 339i$	$-4{\cdot}88 \pm 5{\cdot}61i$	$-1313 \pm 387i$
2	$-17{\cdot}96 \pm 512i$	$-74{\cdot}6 \pm 498i$	$5{\cdot}08 \pm 3{\cdot}80i$	$-720 \pm 302i$

technique. However, to optimize actuator power consumption and damping of the desired modes, linear quadratic regulator (LQR) and Gaussian (LQG) algorithms [26] are used to obtain optimal control and estimator gains, respectively, so that the spillover effects are not sufficient to destabilize the actively controlled system. To implement the digital controller of modal control algorithm, the controlled mode state-space equations of motion corresponding to equation (12), the gain vector in equation (13) and the modal state estimator need to be transformed to the discrete-time domain [27].

7. NUMERICAL EXPERIMENTS

The performance of the modal control algorithms is examined through a series of numerical experiments. Controller and estimator gains are designed to produce maximum damping of the first two eigenvalues and ensure stability of the closed-loop system in the face of spillover effects. The desired eigenvalues, along with controller and estimator gains are given in Table 4. The desired poles are obtained by using the LQR design to minimize the control gains and to achieve high damping. The LQG design is used to obtain the optimal estimator gains. The main consideration in designing the controller is to minimize spillover problems.

In accordance with the discussion in section 6.1, the disturbance (shaker position) and measurement points are at points 7 and 23, respectively, as shown in Figure 10. The control excitation is applied to the PZT actuator placed in the middle of the upper portion of the three-layer plate. The complete closed-loop control system is shown in Figure 11.

The PZT actuator model is initially designed to activate in both the x and y directions (see Figure 10) and the predicted FRFs are shown in Figure 12 where the FRFs relate the integrated velocity from the accelerometer to the disturbance force derived from the load cell. The FRF simulation results in Figure 13 show the influence of activating the PZT model in the x direction only. The results demonstrate that superior suppression of vibrations is obtained by activating in the x direction only since actuation of the PZT in the y direction is liable to induce excitation of higher modes and thus affect the closed-loop

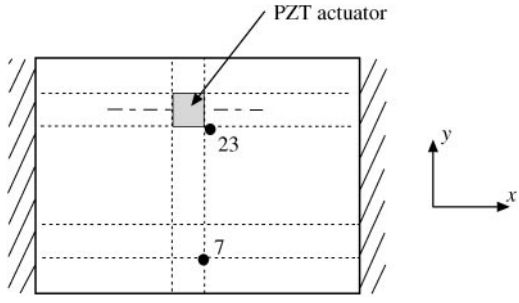

Figure 10. Actuator location and excitation and measurement points (7,23) used in simulation of active constrained layer damping.

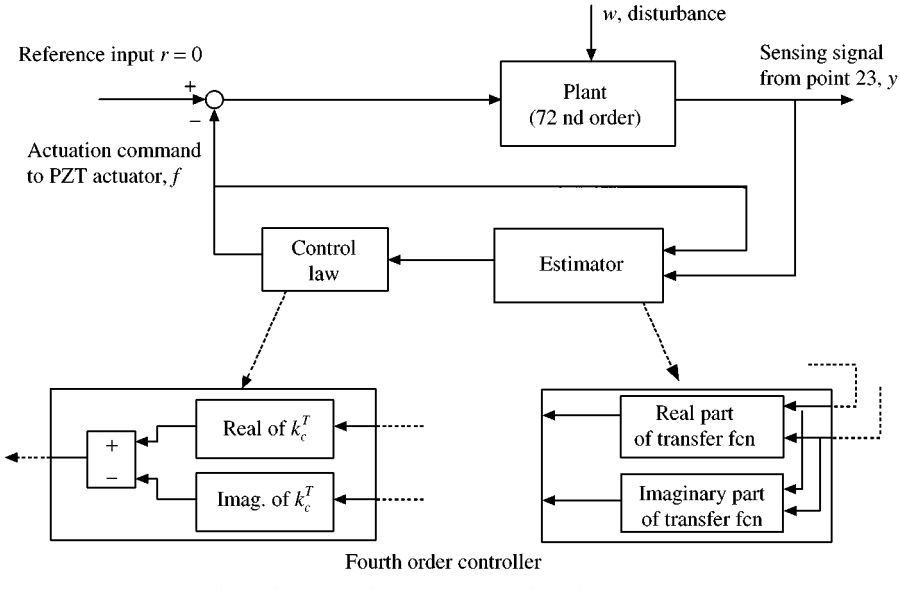

Figure 11. Block diagram of digital control simulation to match with real-time interface using SIMULINK software.

poles. In addition, the power consumption for the PZT actuator decreases when actuation is in one direction only, as shown by the plots of applied voltage versus time in Figure 14 where the disturbance time history is swept sine with a frequency range from 0 to 600 Hz. Also superimposed in Figures 12 and 13 are simulation results produced using a controller designed upon the basis of the reduced order model prior to updating. In both cases the use of the updated model produces superior suppression of the first two modes. Also in Figure 12 there are indications of spillover causing excitation of the modes at around 200 and 500 Hz. Given these results it was decided to proceed with the experimental study using the updated, reduced order model as the basis for controller design.

8. EXPERIMENT FACILITY AND RESULTS

The general arrangement of the test facility is shown in Figure 15. Implementation of the digital controller is performed using a commercial package ("dSPACE" DS1102) which uses

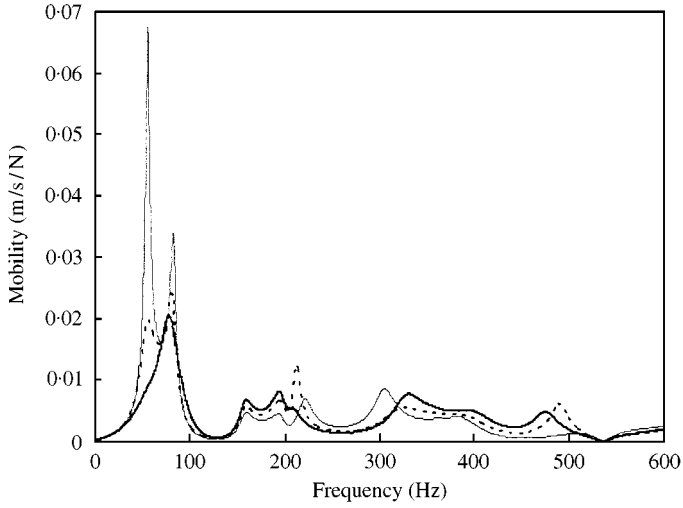

Figure 12. Simulation results: predicted FRFs of three-layer plate with and without active control for PZT actuator operating in both x and y directions: ——, passive control; ———, active control with updated-model controller; - - - - -, active control with erroneous-model controller.

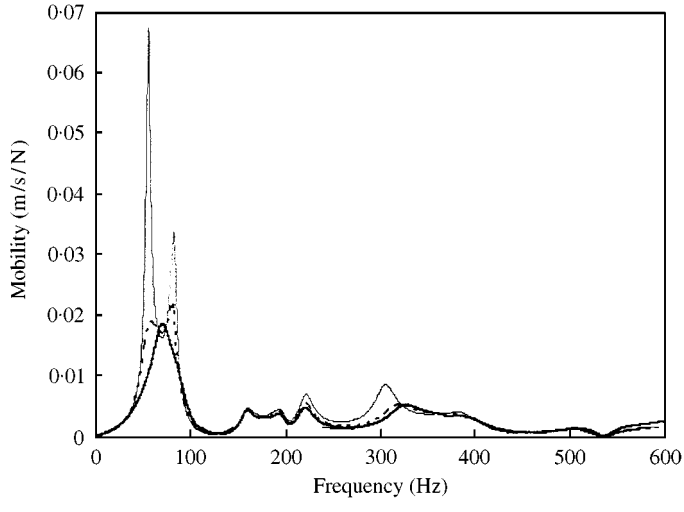

Figure 13. Simulation results: predicted FRFs of three-layer plate with and without active control for PZT actuator operating in x direction only: ——, passive control; ———, active control with updated-model conrtroller; - - - - -, active control with erroneous-model controller.

one analogue-to-digital input channel and one digital-to-analogue output channel. In general, to avoid aliasing of a sampled signal, the sampling frequency must be greater than twice the highest natural frequency, which in this case is around 600 Hz [25]. In the present study it was found that a sampling frequency of 10 kHz provided a suitable compromise between sufficiently accurate discretization of the analogue signal for real-time control and the capabilities of the digital signal processor. This sampling rate also ensures that the spillover effects from the uncontrolled higher frequency modes will not occur. The control interface card is designed to operate with SIMULINK software [28]. Processing of the

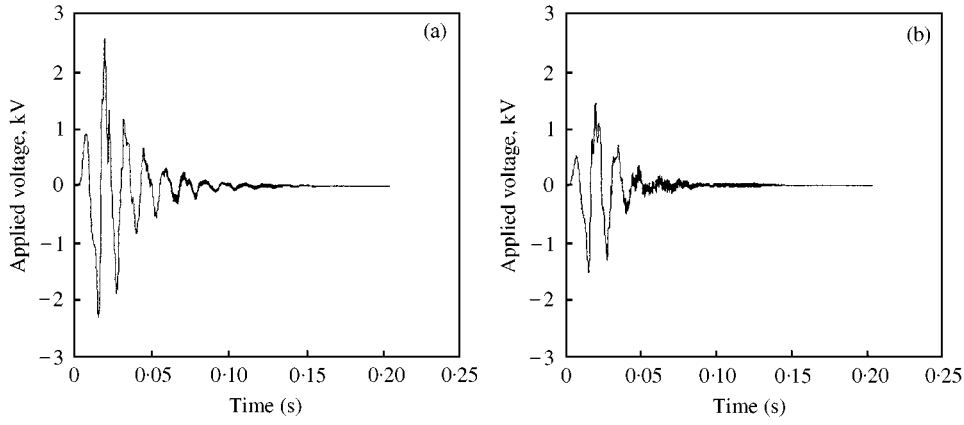

Figure 14. Simulation results: applied voltage for PZT actuator: (a) operating in both x and y directions; (b) operating in x direction only.

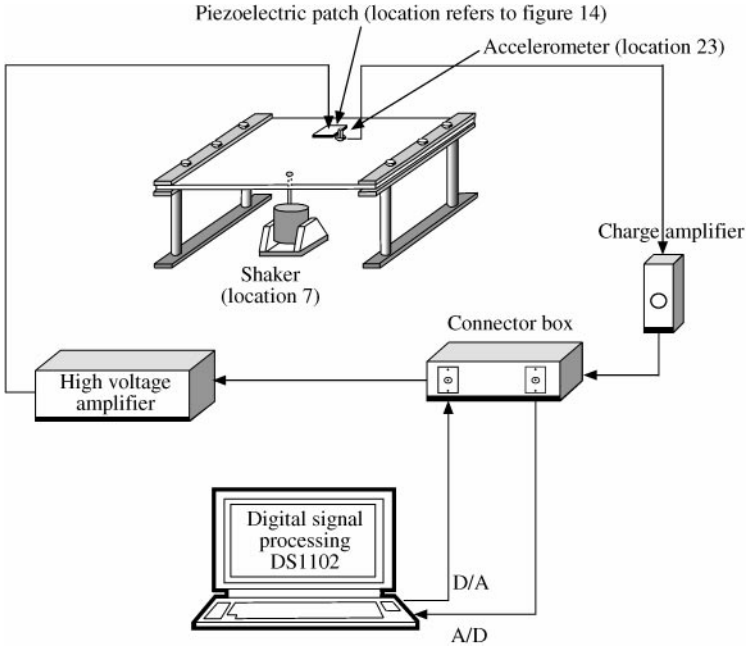

Figure 15. Arrangement of clamped–clamped plate with electronic equipment for digital control implementation.

sensor signal to compute the command force is written in block diagram form in SIMULINK. This programming format is restricted to operations in real numbers and hence the complex matrices of the state-space controller have to be transformed into complex transfer functions (see Figure 11). Real and imaginary terms can then be computed separately in terms of real numbers.

To activate the PZT actuator in the x direction only, a $50\,\text{mm} \times 50\,\text{mm}$ element of PZT material is cut into four strips of equal width and attached to the plate as shown in Figure 16. The PZT actuator is approximately 1 mm thick to react effectively to

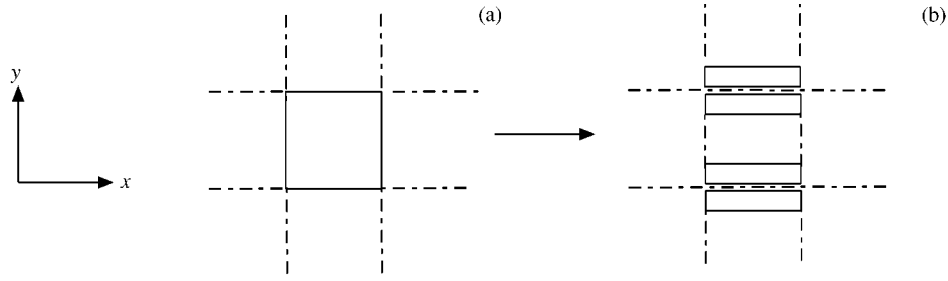

Figure 16. Configuration of PZT actuator: (a) for operation in x and y directions; (b) for operation in x direction only.

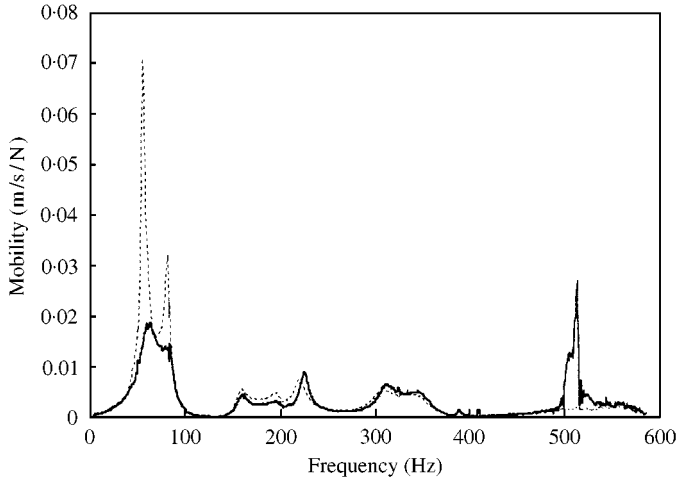

Figure 17. Measured FRFs of three-layer plate with and without active control for PZT actuator operating in both x and y directions: ·····, passive control; ———, active control.

a maximum voltage of from 1 to 2 kV [29]. The relationship between force and voltage applied for the PZT actuator is derived as [29]

$$f(t) = \sigma_a A_a = \left(E_a \frac{d_{31}}{t_a} V(t) \right) b_a t_a$$

$$= -0{\cdot}702\ V(t)\ (\mathrm{N/V}), \tag{14}$$

where σ_a is the stress developed in the PZT, A_a is the cross-section of the PZT, b_a is the width of the PZT, t_a is thickness of the PZT, E_a is the modulus of elasticity of the PZT ($= 1/15{\cdot}1 \times 10^{-12}\ \mathrm{N/m^2}$) and d_{31} is the piezoelectric constant ($= -212 \times 10^{-12}\ \mathrm{m\,V^{-1}}$).

Figures 17 and 18 show FRFs from experiments for different PZT actuator configurations and can be compared directly with the simulation results shown in Figures 12 and 13. Close agreement between simulations and experiments is evident. The introduction of active control results in significant attenuation of the two lowest modes, which was predicted by the simulation results. However the simulation results in Figures 12 and 13 indicated that these two modes would coalesce into a single mode. This did not happen in practice with the modes remaining distinct. The experimental results also show

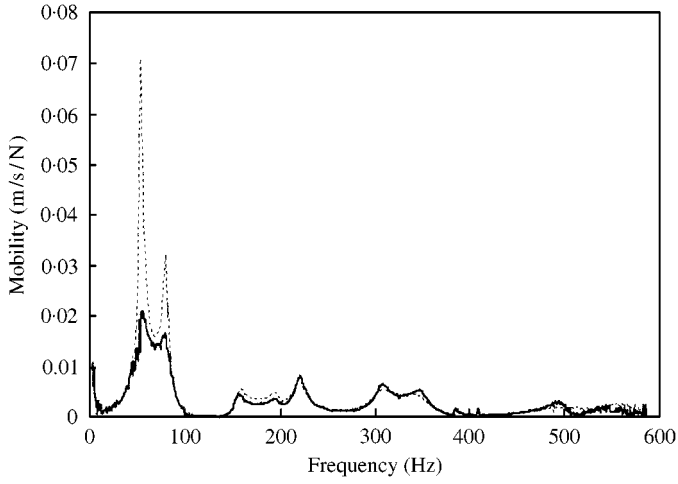

Figure 18. Measured FRFs of three-layer plate with and without active control for PZT actuator operating in x direction only: ·····, passive control; ———, active control.

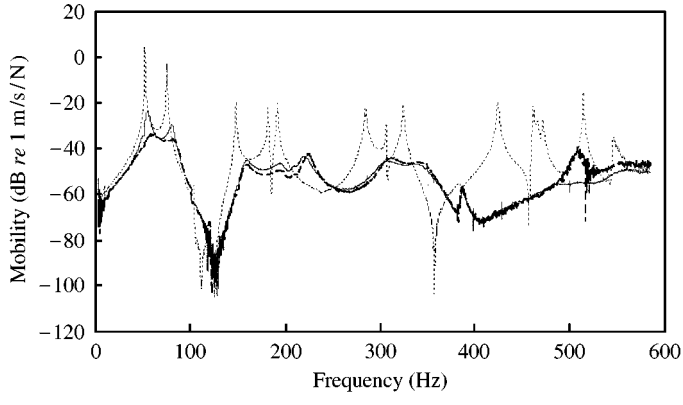

Figure 19. FRF7_23 (PZT operating in two directions): ·····, Bare plate; ———, plate with passive damping layer; - - - - -, plate with active damping control.

the excitation of the mode just above 500 Hz which occurs when the actuator is arranged to operate in both x and y directions.

Comparisons of both active and passive control schemes in relation to the response of the bare plate are shown in Figures 19 and 20. The notation used here is FRFj_k where j is the excitation point and k is the measurement point, as defined in Figure 6. The FRF of the actively damped plate using the two-direction PZT actuator is shown in Figure 19 and Figure 20 is of the one-direction PZT case. The attenuation of the first and second modes is increased through the active damping control by about 10 and 5 dB respectively. Noise is associated with the FRFs measured from the response of the actively controlled plate using the one-direction PZT actuator, especially at low and high frequencies. This may arise from the unsynchronized operation of the four-strip PZT actuator designed to operate in one direction only. The results in Figures 19 and 20 show clearly the influence of passive and active constrained layer damping on the dynamic response of the plate.

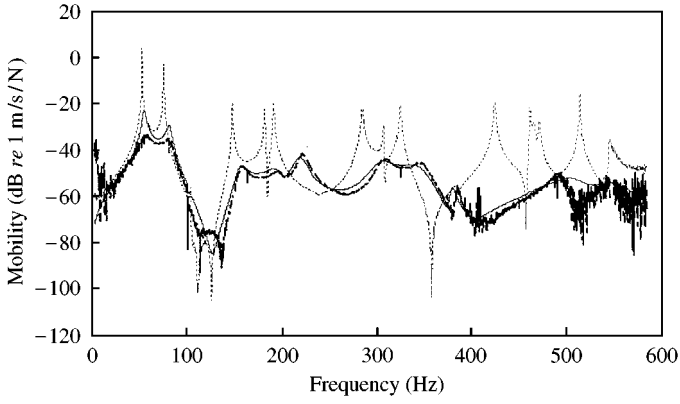

Figure 20. FRF7_23 (PZT operating in two directions): ·····, Bare plate; ———, plate with passive damping layer; - - - - -, plate with active damping control.

9. CONCLUSIONS

In this paper, the authors have described both numerical and experimental investigations into the active constrained layer damping of a clamped–clamped plate. The strategy adopted has involved the development of a model-based approach to control system design. The aim has been to minimize the amount of control hardware required whilst avoiding spillover problems which are liable to degrade performance.

Initially, a passive constrained damping layer was introduced and its influence on vibration levels was investigated. Not unexpectedly it was found that the higher modes benefited significantly from the introduction of the passive layer: modes 3–10 in the range from 150 to 600 Hz were attenuated by approximately 25 dB. The first two modes (bending, torsional) below 100 Hz were attenuated by a similar amount. However, peak mobility levels for modes 1 and 2 were still some 20 dB above those of the higher order modes and an active strategy was developed to deal with this problem.

The development of the active control system involved the transformation of the original finite element model of the plate into a modal state-space description to be implemented in discrete time. To illustrate some of the key problems involved in this transformation and the solutions which were devised, the mathematical treatment has been described in some detail. The end result of the various computations was a fourth order estimator/controller. Numerical experiments indicated that such an arrangement was capable of attenuating modes 1 and 2 (in conjunction with a 72nd order model of the plate) without incurring problems due to spillover. This was achieved using only a single sensor and single actuator channel.

The experimental study confirmed the results of the numerical simulations. Two configurations of actuator were investigated—a single PZT patch arranged to provide actuation in mutually perpendicular directions, and an arrangement of four PZT patches driven by a single amplifier but designed to activate the plate in a single direction only. Both configurations were effective at controlling modes 1 and 2 but the single PZT patch produced significant excitation of a mode above 500 Hz.

Two mobility/frequency plots have been used to summarize the effects of passive and active constrained layer damping and actuators operating in one and two directions. By using the four-patch arrangement the excitation of the mode above 500 Hz, which occurs using a single patch, can be avoided. Also, using the four PZT patches collocated with the sensor produces the greatest attenuation of modes 1 and 2 but the mobility/frequency plot is

noisier, especially at high and low frequencies. Overall, the experiments show that the passive layer introduces sufficient damping into the higher modes to avoid any serious problems due to spillover effects.

Future work will be aimed at comparing the performance of the time-domain control algorithm with robust frequency domain methods which have recently been developed for use with plate-like structures [30].

ACKNOWLEDGMENTS

The authors would like to thank the European Research Office of the US Army for partial funding of the control equipment under contract no. N68171-98-M-5388.

REFERENCES

1. M. J. Balas 1978 *IEEE Transactions on Automatic Control* **AC-23**, 673–679. Feedback control of flexible systems.
2. L. Meirovitch, H. Baruh and H. Oz 1983 *Journal of Guidance and Control* **6**, 302–310. A comparison of control techniques for large flexible systems.
3. T. Bailey and J. E. Hubbard Jr 1985 *Journal of Guidance and Control* **8**, 605–611. Distributed piezoelectric-polymer active vibration control of a cantilever beam.
4. J. L. Fanson and T. K. Caughey 1990 *American Institute of Aeronautics and Astronautics Journal* **28**, 717–724. Positive position feedback control for large space structures.
5. A. Baz, S. Poh and J. Fedor 1992 *American Society of Mechanical Engineers Journal of Vibration and Acoustics* **114**, 96–103. Independent modal space control with positive position feedback.
6. A. Baz and J. Ro 1993 *Conference of Engineering Sciences Society, Charlottesville, VA*. Partial treatment of flexible beams with active constrained layer damping.
7. A. Baz and J. Ro 1996 *Smart Materials and Structures* **5**, 272–280. Vibration control of plates with active constrained layer damping.
8. D. E. Veley and S. S. Rao 1996 *Smart Materials and Structures* **5**, 660–671. A comparison of active, passive and hybrid damping in structural design.
9. B. Azvine, G. R. Tomlinson, R. J. Wynne and O. Sensburg 1994 *Fourth International Conference on Adaptive Structures, Cologne*. Vibration suppression of flexible structures using active damping.
10. R. Firoozian and R. Stanway 1988 *Mechanical Systems and Signal Processing* **2**, 243–264. Active vibration control of turbomachinery: a numerical investigation of modal controllers.
11. P. Avitabile, J. O'callahan and J. Milani 1989 *Seventh IMAC*, 1109–1115. Comparison of system characteristics using various model reduction techniques.
12. J. E. Mottershead and M. I. Friswell 1993 *Journal of Sound and Vibration* **167**, 347–375. Model updating in structural dynamics: a survey.
13. T. P. Khatua and Y. K. Cheung 1973 *International Journal for Numerical Methods in Engineering* **6**, 11–24. Bending and vibration of multilayer sandwich beams and plates.
14. D. J. Dawe 1984 *Matrix and Finite Element Displacement Analysis of Structures*. New York: Oxford University Press.
15. C. Chantalakhana and R. Stanway 1998 *Proceedings of the Fourth European and Second MIMR Conference, Harrogate, U.K.*, 195–204. Control of plate vibrations using smart technology.
16. D. Ross, E. E. Ungar and E. M. Kerwin Jr 1959 *Structural Damping, Sec.* 3, *The American Society of Mechanical Engineers*. Damping of plate flexural vibrations by means of viscoelastic laminae.
17. D. J. Inman and C. Minas 1990 *Control and Dynamic Systems* **37**, 327–363. Matching analytical models with experimental modal data in mechanical systems.
18. B. Porter and R. Crossley 1972 *Modal Control Theory and Applications*. London: Taylor & Francis.
19. C. Minas and D. J. Inman 1989 *Transactions of the American Society of Mechanical Engineers, Journal of Vibration and Acoustics* **113**, 219–224. Identification of a nonproportional damping matrix from incomplete modal information.

20. R. J. GUYAN 1965 *American Institute of Aeronautics and Astronautics Journal* **3**, 380. Reduction of stiffness and mass matrices.
21. V. N. SHAH and M. RAYMUND 1982 *International Journal for Numerical Methods in Engineering* **18**, 89–98. Analytical selection of masters for the reduced eigenvalue problem.
22. M. I. FRISWELL and J. E. MOTTERSHEAD 1995 *Finite Element Model Updating in Structural Dynamics*. The Netherlands: Kluwer Academic Publishers.
23. D. J. EWINS 1986 *Modal Testing: Theory and Practice*. Herts, England: Research Studies Press Ltd.
24. LMS 1993 *LMS CADA-PC* User Manual.
25. G. F. FRANKLIN, J. D. POWELL and M. WORKMAN 1998 *Digital Control of Dynamic Systems* CA, U.S.A.: Addison-Wesley Longman, Inc.; third edition.
26. J. B. BURL 1999 *Linear Optimal Control*. CA, U.S.A.: Addison-Wesley Longman, Inc.
27. K. OGATA 1987 *Discrete-time Control Systems*. London: Englewood Cliffs, Prentice-Hall.
28. J. B. DABNEY and T. L. HARMAN 1996 *The Student Edition of SIMULINK*. Englewood Cliffs, NJ: Prentice-Hall.
29. Physik Instrumente (PI) Tutorial Manual. 1999 *Web page*: *http://www.physikinstrumente.com/tutorial*.
30. A. M. SADRI, R. J. WYNNE and J. R. WRIGHT 1999 *Proceedings of the Institution of Mechanical Engineers*. **213**, 489–504. Robust strategies for active vibration control of plate-like structures: theory and experiment.

APPENDIX A: NOMENCLATURE

A_a	cross-sectional area of the PZT actuator (m^2)
b_a	width of the PZT actuator (m)
$\mathbf{B}_0$	input matrix ($n \times n$)
$\mathbf{C}$	measurement matrix ($2m \times 2n$)
d_{31}	piezoelectric constant (m/V)
e_{13}	ratio of the modulus of elasticity between the constraining layer and the base plate
$E_{1,3}$	modulus of elasticity of the constraining layer and the base plate respectively (N/m^2)
E_a	modulus of elasticity of the PZT actuator (N/m^2)
$f(t)$	force varied in time (N)
$\mathbf{f}$	input vector ($n \times 1$)
G	modulus of rigidity (N/m^2)
$\mathbf{G}$	gain matrix ($n \times 2m$)
$h_{1,2,3}$	thickness of the constraining layer, viscoelastic and base plate respectively (m)
h_{23}, h_{13}	thickness ratio between the viscoelastic layer and the base plate and the constraining layer and the base plate respectively
$\mathbf{I}$	identity matrix ($r \times r$)
i, j, k, l, m, n, r	integer
$\mathbf{M}_j$, $\bar{\mathbf{K}}_j$	mass and complex stiffness matrices for the jth element (kg, N/m^2)
$\mathbf{M}$, $\mathbf{D}$, $\mathbf{K}$	global mass, damping and stiffness matrices ($n \times n$)
$\mathbf{M}^R$, $\bar{\mathbf{K}}^R$	reduced-order mass and complex stiffness matrices ($r \times r$)
t	time
t_a	thickness of the PZT actuator (m)
$u_{1k,3k}$	longitudinal displacement in x-axis at node k of the rectangular element of the constraining layer and the base plate respectively (m)
$\mathbf{U}$	eigenvector matrix ($2r \times 2r$)
$v_{1k,3k}$	longitudinal displacement in y-axis at node k of the rectangular element of the constraining layer and the base plate respectively (m)
$V(t)$	applied voltage across the PZT actuator (V)
w_k	transverse displacement in z-axis at node k of the rectangular element (m)
$\frac{\mathrm{d}w}{\mathrm{d}y_k}$, $\frac{\mathrm{d}w}{\mathrm{d}x_k}$	rotational displacement about x- and y-axis respectively (rad)
$\mathbf{Y}$	state vector ($2r \times 1$)
$\mathbf{Z}^R$, $\mathbf{K}^R$	reduced order imaginary and real terms, respectively, of the complex stiffness matrices ($r \times r$)
η	loss factor of viscoelastic layer

v_3	Poisson's ratio of the base plate
ρ_3	density of the base plate (kg/m^3)
σ_a	stress developed in the PZT actuator (N/m^2)
$\boldsymbol{\xi}$	modal co-ordinate vector ($2r \times 1$)
$\boldsymbol{\Lambda}$	eigenvalue matrix ($2r \times 2r$)
$\boldsymbol{\Delta}_j$	displacement vector of the rectangular element j (28×1)
$\boldsymbol{\Delta}\mathbf{A}_{1,2}$	mass-normalized correction matrices for the damping and stiffness matrices respectively
i	complex operator, $\sqrt{-1}$
$[\ ]^{\mathrm{T}}$	matrix transpose
$[\ ]^{-1}$	matrix inverse
$[\ ]^*$	complex conjugate matrix transpose
$[\ ]_c$	controlled terms
$[\ ]_u$	uncontrolled terms
$[\dot{\mathbf{x}}]$	differentiation of $\mathbf{x}$ variable with respect to time